Extracting the Group Index of a Silicon Waveguide from the Free Spectral Ranges of Integrated Interferometers

Kevin-E

I. Introduction

WITHIN the scope of the Silicon Photonics Design, Fabrication and Data Analysis online course, this project is intended to introduce us to the fundamental workflow of designing and simulating integrated photonic circuits, and later comparing the measured, real-world optical throughput to our design intents and simulation results. The specific aim of this project is to design a set of passive interferometers which allow to gain insights into the propagation of light within the silicon waveguides.

As of now, this proposal introduces the concept of the group index, the working principle of unbalanced passive interferometers and how the group index can be extracted from the free spectral range (FSR) of the latter. Soon, the layout for the proposed circuits will be designed and the circuits will be manufactured using modern electron beam lithography. The technology platform we rely on during this project is silicon photonics, which means we are using silicon waveguides within a silicon oxide cladding, which is a mature and widely used platform for photonic integrated circuits in the infrared regime.

All derivations presented here are a summary of the course lectures and can be read in [1].

II. Theory

A. Light propagation within a waveguide

An optical waveguide is a material with a higher index of refraction than its immediate surroundings, and is usually shaped like a long cylinder or strip in order to facilitate the propagation of light along one direction while confining it in the other two dimensions. For finite waveguide cross sections, the Maxwell equations exhibit only discrete solutions, which are referred to as waveguide modes. These are categorized by the direction of the electric field, which remains constant along the direction of propagation, and allows to distinguish between (quasi) transverse electric (TE) and (quasi) transverse magnetic (TM) modes, of which there are a fundamental and infinitely many higher modes. Depending on the size of the waveguides cross section, only few modes are guided and actually propagating whereas the others are radiating out. For this project, we only consider single-mode waveguides which are so small that they guide only the fundamental modes.

Two important figures of merit of a waveguide are its effective index of refraction and the group index. Since the cross-sectional field profile depends on the waveguide geometry (and the mode in question), and in particular the fraction of the light that is confined to the waveguide itself as opposed to the surrounding cladding, the index of refraction that is experienced by the mode is not just that of the waveguide material. In order to determine this effective index which actually determines the phase velocity, we were instructed to perform numerical calculations using the commercial software Lumerical. For this project, I choose to stick with the default waveguide size provided by the SiEPIC PDK, *i.e.*, a silicon strip waveguide which is 500 nm wide and 220 nm thick. The simulation result for the cross-sectional field profile of the fundamental TE mode at 1550 nm is presented in Fig. 1. By varying the wavelength, the simulation also yields the wavelength dependence of this effective index of refraction, which can be fitted by a second-order Taylor series around the center wavelength $\lambda_0 = 1550\,\mathrm{nm}$:

$$n_{\mathrm{eff}}(\lambda) = 2.447 - 1.133 \cdot (\lambda - \lambda_0) - 0.0411 \cdot (\lambda - \lambda_0)^2. \quad (1)$$

This effective index is now used to describe the propagation of this mode along the z direction in a simple plain wave formalism with the amplitude

$$E(x, y, z) = E(x, y, z_0) \cdot \exp\left(-i\beta(z - z_0)\right) \quad (2a)$$

$$\beta = \frac{2\pi n_{\mathrm{eff}}}{\lambda_0} - i\alpha \quad (2b)$$

with the cross-sectional mode profile $E(x, y, z_0)$, the propagation constant β, the vacuum wavelength λ_0 and the attenuation constant α.

One significant consequence of the fact that the index of refraction varies for different wavelengths, is that a short light pulse, which is inherently composed of an extended wavelength range, does not propagate with the same velocity as the phase of the electromagnetic field, since all its wavelength components propagate at different velocities. The propagation velocity of the wave packages envelope, dubbed the *group velocity* v_g, rather depends on the wavelength dependence of the refractive index and can, in a first-order approximation, be expressed as

$$v_g = \frac{c}{n - \lambda \frac{\partial n}{\partial \lambda}} \equiv \frac{c}{n_g} \quad (3)$$

with the group index n_g. This group velocity physically describes how fast energy and information is actually propagating through the waveguide and is, therefore, of utmost importance for a variety of photonic circuits. Since $\partial n/\partial \lambda$ is negative in a silicon waveguide according to Eq. 1, the group

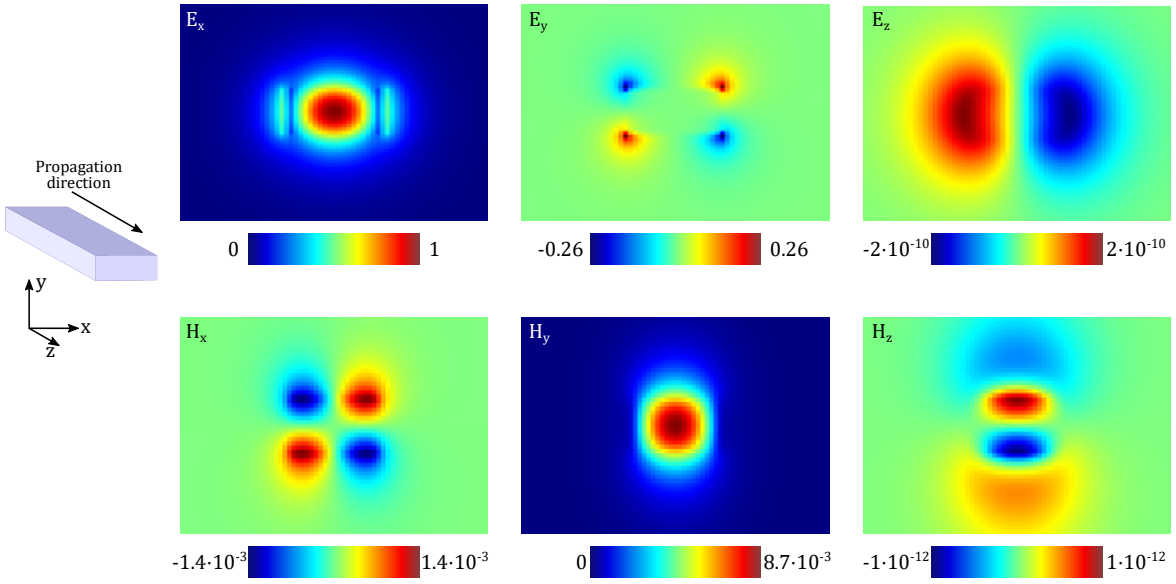

Fig. 1. Electric field components of the fundamental quasi TE mode of the 500 nm × 220 nm silicon waveguide with silica cladding. The electric field is mostly oriented along the x direction whereas the magnetic field is mostly oriented along the y direction.

velocity is slower than the phase velocity. For the case of the strip waveguide which is to be used in this project, a simulation in LUMERICAL MODE yields a group index of $n_g = 4.203$ for the fundamental TE mode.

B. Unbalanced interferometers

An interferometer is used to determine the phase difference between two light waves by exploiting the fact that merging two waves is a vector summation which may result in constructive or destructive interference and, hence, in a measurable amplitude variation as a function of the phase difference. For this project, we will consider two different interferometer topologies: the Mach-Zehnder interferometer (MZI) and the Michelson interferometer (MI).

The MZI works by splitting an incoming light wave into two beams, propagating them individually along two independent paths — in our case, two different waveguides — and merging them again at an output port. At the latter, the two waves may exhibit a phase difference depending on whether their optical path lengths were different or whether they propagated through media with different indices of refraction. This can be expressed as a change of either z or β in the exponent of Eq. 2. Here, we will not alter n_{eff} and assume no losses (hence, $\beta_1 = \beta_2 \equiv \beta$) but will instead focus on introducing an optical path difference ΔL, thereby rendering the interferometer *unbalanced*. The only accessible quantity during an experiment, namely the light intensity at the output, can finally be expressed as

$$I_{\text{out}} = \frac{I_{\text{in}}}{4}\left|\exp\left(-i\beta L_0\right) + \exp\left(-i\beta(L_0+\Delta L)\right)\right|^2 \quad (4)$$

$$= \frac{I_{\text{in}}}{2}\Big(1+\cos\left(\beta\cdot\Delta L\right)\Big). \quad (5)$$

At fixed ΔL, this exhibits an oscillating behavior with regard to $1/\lambda$. The periodicity of this throughput oscillation in terms of the wavelength is dubbed the free spectral range (FSR) and constitutes a key parameter of such an interferometer. In a first-order approximation it can be simplified as

$$\text{FSR} = \Delta\lambda = \frac{\lambda^2}{\Delta L \cdot n_g}. \quad (6)$$

As a conclusion, the group index n_g can be deduced by measuring the wavelength-dependent throughput of an MZI and calculating its FSR. A plot of $\text{FSR}(\Delta L)$ can then be fitted by a function $y = a/x$ whereas the fit parameter a depends on the wavelength — which is known — and n_g.

The Michelson interferometer works in a similar fashion: an incoming wave is split into two beams which then propagate through two different waveguides. In contrast to the MZI, the two waves are then reflected at the end of their respective optical path and combined again in the same component that was also used to split the incoming beam. In a free-space optical setup, this is usually realized by using a semi-transparent mirror. In integrated optics, the same can be achieved by using a so-called directional coupler, which is a four-port component that acts as a two-way beam splitter and combiner. An expression for the light intensity at the output

TABLE I
CALCULATED AND SIMULATED FREE SPECTRAL RANGES OF THE PROPOSED MACH-ZEHNDER AND MICHELSON INTEROMETERS AROUND A CENTER WAVELENGTH OF 1550 NM.

Mach-Zehnder			Michelson	
ΔL (µm)	Calc. FSR (nm)	Simul. FSR (nm)	ΔL (µm)	Simul. FSR (nm)
19	30.09	30.02	9.5	34.05
22.8	25.07	25.02	11.4	27.79
30	19.05	19.19	15	20.81
40	14.29	14.3	20	15.22
60	9.53	9.48	30	9.84
120	4.76	4.72	60	4.87
230	2.49	2.49	115	2.51
300	1.91	1.91	150	1.92

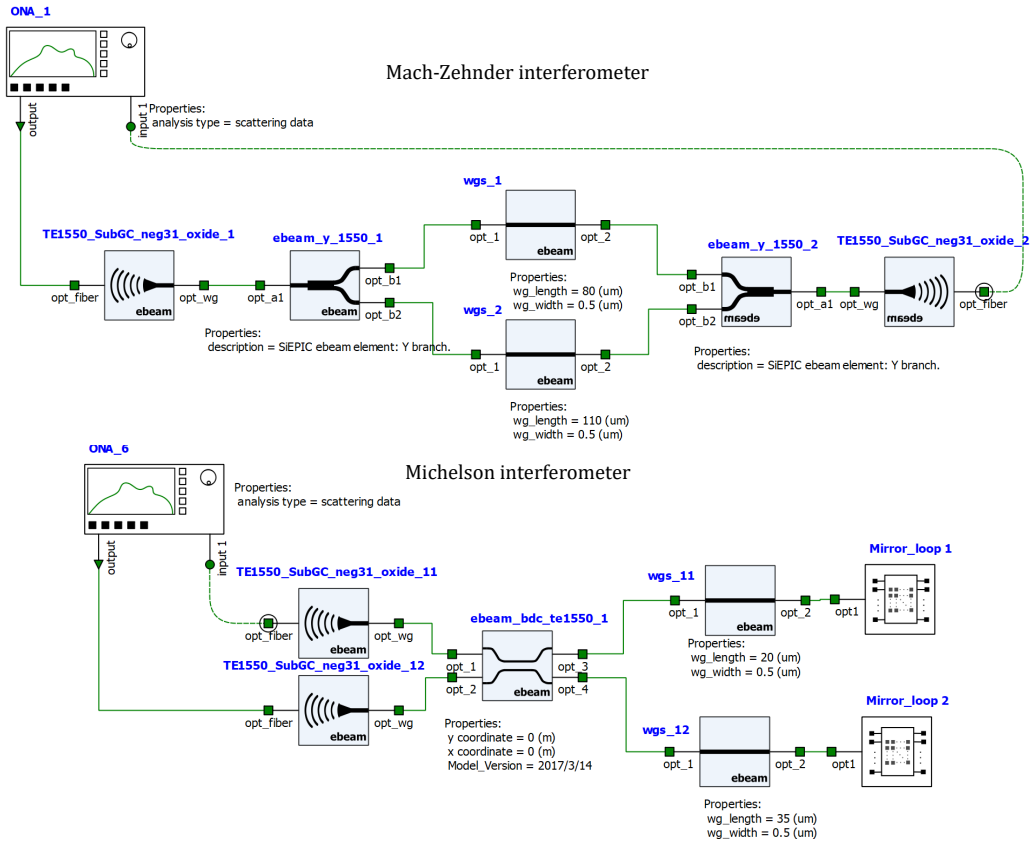

Fig. 2. LUMERICAL INTERCONNECT circuit models of the proposed Mach-Zehnder and Michelson interferometers.

of the directional coupler can be deduced in the very same fashion as was done above for the MZI. The only difference is that the light passes each branch twice. Hence, Eq. 6 still holds for an MI if the path difference in the denominator is amended by a factor of two.

III. CIRCUIT PROPOSAL

For this project, I want to explore and compare the MZI and the MI topologies and propose designing and manufacturing eight of each with different branch length differences ΔL. Due to the limited time budget that I can dedicate to this course at the moment, I choose to implement each interferometer using the components which are conveniently provided by the SiEPIC PDK, complete with layouts and component models for LUMERICAL INTERCONNECT.

For both interferometers, I must now choose two key parameters, namely the length of the reference branch L_0 and the path difference ΔL. I begin with the Mach-Zehnder interferometer. Considering the predetermined distance of the grating couplers, which must fit the fixed distance of the probe fibers used to couple laser light into and out of the chip, as well as the length of the required Y-splitter components and two quarter waveguide bends for connecting the grating couplers, a reference length of 80 µm is chosen. This length will be kept constant for all variants, whereas ΔL will be varied among the eight implementations. In order to nicely cover the experimentally accessible wavelength range, the path differences listed on the left of Tab. I are chosen. In this table, also the corresponding FSR is given according to Eq. 6 while assuming a group index of 4.203 as obtained by the simulation presented in Sec. II-A. The expected FSR varies between roughly 2 and 30 nm, which will be easily measurable considering the 50 nm bandwidth of the grating couplers and the 0.01 nm wavelength resolution. At the same time, these path length differences are easily implemented by waveguide snakes while respecting the maximum available chip space.

For the Michelson interferometers, each waveguide branch is passed by the light twice, so I adapt the parameters chosen for the MZIs above by dividing them by two. Also taking into account the roughly 40 µm round-trip at the mirror loops at the end of each branch yields a reference path length of 20 µm and the path differences listed on the right of Tab. I.

Finally, all interferometer circuits are implemented in LUMERICAL INTERCONNECT as presented in Fig. 2. As mentioned before, I did not have the time to design my own components but instead rely on the provided component models. An optical network analyzer is connected to the grating coupler components in order to inject light into the circuit and analyze the output. For the MZI, the light is split and combined using Y-branches, and for the MI, the provided broadband directional coupler is chosen to split and combine the light, whereas the standard Y-branches are used to implement the mirror loops terminating each optical path.

For implementing the mirror loops, the exit ports of the Y-splitter as provided by the PDK are too closely spaced to allow for a direct half-circle connection with a radius of 5 µm.

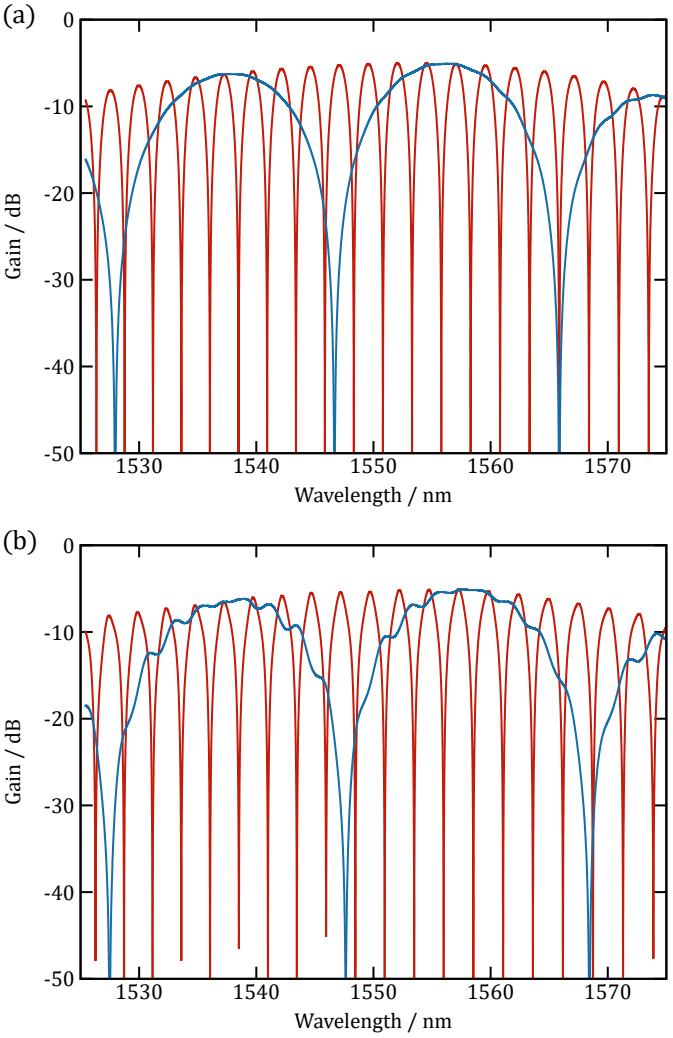

Fig. 3. Simulated thoughput of the (a) Mach-Zehnder and (b) Michelson interferometers. The blue lines correspond to $\Delta L = 30\,\mu\text{m}$ (15 µm) and the red lines to $\Delta L = 230\,\mu\text{m}$ (115 µm), respectively.

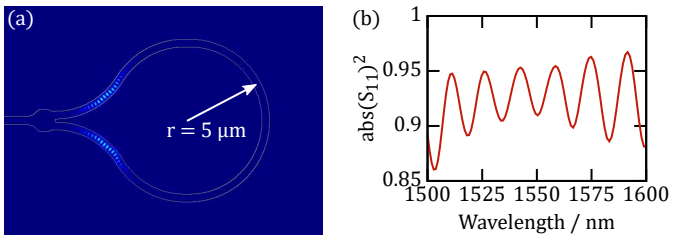

Fig. 4. Mirror loop for terminating the optical paths of the Michelson interferometers using a modified Y-splitter. (a) Device outline and snapshot of a propagating wave package as simulated by 3D FTDT. (b) Wavelength dependence of the absolute reflectivity, *i.e.*, $|\text{S}_{11}|^2$.

Hence, the output waveguides of this splitter were replaced by custom S-curves with a 5 µm bend radius which attach directly to the multimode expansion region of the splitter and widen up the output port distance to exactly 10 µm. From this point, the loop can be closed by a half-circle as can be seen the device outline in Fig. 4(a). This way, the footprint of this component is minimized while maintaining a constant 5 µm bend radius. The resulting component was simulated

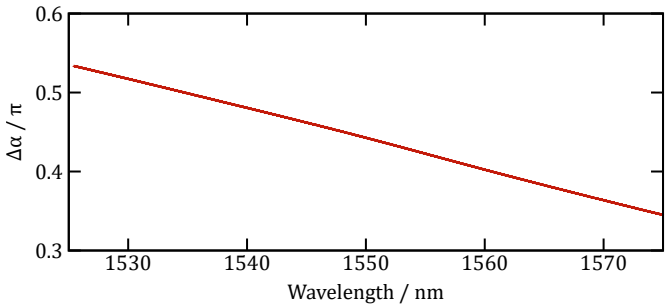

Fig. 5. Phase difference of waves exiting ports 3 and 4 of the PDKs broadband directional coupler when injecting light at port 1.

using 3D FTDT which resulted in the screenshot of the wave package propagation presented in Fig. 4(a) as well as the S-parameter of this one-port device, which is then imported into LUMERICAL INTERCONNECT. Its squared absolute value is plotted in Fig. 4(b) and exhibits a vague oscillating wavelength dependence reminiscent of a cavity resonance.

Fig. 3 exemplarily presents the simulated throughput of both interferometer topologies for one small and one large value of ΔL, respectively. The oscillatory throughput behavior can be clearly observed, and the free spectral range was extracted from the data at adjacent dips closest to 1550 nm and added to Tab. I. The simulated FSR values of the MZI are in remarkable agreement to the values obtained using Eq. 6, whereas the MI throughput seems to exhibit more ripples and a slightly larger deviation from the ideal FSR, especially for small values ΔL and correspondingly large FSR. The latter is probably to be attributed to the broadband directional coupler used to split the input beam since it introduces a wavelength dependent phase difference between the two output beams, which is plotted in Fig. 5. This shift is added to the phase shift obtained by the optical path length difference in the interferometer branches, and shifts the wavelength of, *e.g.* transmission dips depending on their position in the spectrum. This obviously affects the distance of two dips more if they are further apart in terms of wavelength.

At last, I would also like to implement a few simple component test circuits in which *e.g.* two grating couplers are connected directly to each other, and another in which each port of a Y-splitter is directly connected to a grating coupler. This way I can compare the results of the component simulations to experimental data as well and will be able to subtract out the losses of the couplers.

REFERENCES

[1] L. Chrostowski and M. Hochberg, *Silicon Photonics Design: From Devices to Systems*. Cambridge University Press, 2015.